Flow Turbulence Combust (2015) 94:79–95
DOI 10.1007/s10494-014-9582-0

An Experimental Investigation of Turbulent Convection Velocities in a Turbulent Boundary Layer

Callum Atkinson · Nicolas Alexander Buchmann · Julio Soria

Received: 30 December 2013 / Accepted: 30 October 2014 / Published online: 20 December 2014

Abstract Turbulent convection velocities in a turbulent boundary layer at a Reynolds number of $Re_\theta = 2250$ are examined via the use of a high repetition rate particle image velocimetry measurement undertaken in a water tunnel. Multiple cameras are used to improve the spatial dynamic range of the measurement and reduce the bias towards large-scale structures while simultaneously capturing a wall-normal domain of 0.06δ to 1.7δ. The impact of measurement noise is minimized via careful temporal and spatial filtering of the velocity fields as guided by the comparison of temporal and spatial velocity power spectra with spatially filtered direct numerical simulation data, enabling an estimation of the effective noise-limited spatial and temporal dynamic range of the present experimental measurement. Space-time correlations and phase-spectra are used to estimate the mean and streamwise wave-number dependent convection velocities at various heights above the wall. Results reveal convection velocities greater than the local mean velocity in the lower log layer, decreasing to a level 3.5 % lower than the mean velocity in the upper log and wake regions. The convection velocity is shown to depend on the streamwise length scale and is found to decrease at higher wave-numbers for all wall-normal locations. Comparison between the measured and reconstructed spatial fields show that Taylor's hypothesis can only be applied over short streamwise distances of less than 1δ in the buffer and inner log-layer, while larger projection distances ($\geq 3\delta$) are possible in the outer-log and wake region of the turbulent boundary layer.

Keywords Taylor's hypothesis · Convection velocity · Space-time correlation · Time-resolved PIV

C. Atkinson (✉) · N. A. Buchmann · J. Soria
Laboratory for Turbulence Research in Aerospace and Combustion, Department of Mechanical and Aerospace Engineering, Monash University, Victoria, 3800, Australia
e-mail: callum.atkinson@monash.edu

J. Soria
Department of Aeronautical Engineering, King Abdulaziz University, Jeddah, Kingdom of Saudi Arabia

1 Introduction

Until recently experimental measurements of turbulent flows could generally be divide into either spatially resolved laser diagnostics based measurements [e.g. Particle Image Velocimetry (PIV)] or temporally resolved point measurements [Hot-Wire Anemometry (HWA) or Laser Doppler Anemometry (LDA)]. PIV measurements are typically limited in temporal resolution due to the relatively low firing rates of the lasers ($\approx$ 10 Hz) and the low acquisition rates of the cameras (1 to 30 Hz) that are available for such measurements. In contrast, the field of view and spatial resolution of HWA measurements tend to be limited by the finite size of the probe, conduction effects and potential for these probes to influence the surrounding flow, while LDA measurements are limited by the number of probes that are available for a given measurement. As a result of these experimental limitations the spatial structure and wavelengths associated with turbulence measurements are often inferred from temporal data via the application of Taylor's hypothesis [17] or the frozen turbulence approximation, in which it is assumed that the temporal Eulerian observation of a fixed point in space is approximately the same as the uniform convection of the turbulent flow structure through the same point. Following Townsend [18] this can be expressed as:

$$U(x,t) = U(x - U_c \cdot \Delta t, t + \Delta t), \tag{1}$$

where Δt is the time separation between two measurements and U_c is the turbulent convection velocity. This convection velocity depends on the propagation of turbulent eddies and is therefore highly relevant to the study of the dynamics of turbulence.

In flows that possess a dominant flow direction and velocity, such as jets, pipe flows, channel flows and boundary layers, the general application of Taylor's hypothesis assumes that the convection velocity is equal to the local mean flow velocity and is independent of frequency or wave-number. While this is generally true when turbulent fluctuations u_i' are small with respect to the U_c, previous research has shown that this approximation breaks-down in regions of strong shear [12], where peak production occurs and larger turbulent fluctuations are observed. Assuming that the entire flow and all associated coherent structures convect at the local mean velocity can lead to the misinterpretation of large-scale structures as demonstrated by Zaman and Hussain [22] when examining turbulent jets.

For wall-bounded turbulent flows the convection velocity can be determined as a function of the height above the wall y, and the streamwise k_x and spanwise k_z wave-numbers, if an accurate frequency-wavenumber spectrum $\phi(k_x, k_z, \omega)$ or its Fourier transform, the space-time correlation function, can be determined [20]. Unfortunately both of these are difficult to obtain experimentally, owing to the need to simultaneously measure at a sufficient temporal and spatial resolution, while acquiring records of sufficient length to perform accurate Fourier transforms in each. Recent advances in high-speed digital imaging and the availability of high-speed lasers have seen a renewed interest in the experimental measurement of turbulent convection velocities and its use for extrapolating the three-dimensional structure of the flow [5]. Despite this interest, researchers are yet to provide a complete picture of the effect of wall-normal position and wave-number dependency on the convection velocity of a zero-pressure gradient turbulent boundary layer, with the comparison of results often complicated via the use of different convection velocity estimation methods, along with variations in spatial resolution and different wall-normal positions. A summary of the different fields of view and resolutions is provided in Table 1.

Table 1 Field of view and spatial and temporal resolution of the boundary layer measurements for the investigation of the turbulent convection velocity

Researchers	Plane	Cameras	Field of view (x, y, z)	Resolution $\Delta W_x, \Delta W_y, \Delta W_z, \Delta t$
Krogstad et al. [9]	displaced HWAs			$-, -, 0.005\delta$
$Re_\theta = 1,409$				$-, -, 3^+,$
Dennis and Nickels [4]	streamwise,	2	$6\delta, -, 3\delta$	0.1δ
$Re_\theta = 4,685$	spanwise plane $(x - z)$			
LeHew et al. [11]	streamwise,	2	$10\delta, -, 5\delta$	0.16δ
$Re_\theta = 1,280$	spanwise plane $(x - z)$		$4,712^+, -, 2,356^+$	$74^+, 34^+, 74^+, 0.5^+$
de Kat et al. [2]	streamwise,	2	$2\delta, 0.5\delta, -$	0.007δ
$Re_\tau = 2,700$	wall-normal plane $(x - y)$		$5400^+, 1350^+, -$	$20^+, 20^+, 27^{+\dagger}, 1.5^+$
Present	streamwise,	2	$3.2\delta, 1.7\delta, -$	0.03δ
$Re_\theta = 2,250$	wall-normal plane $(x - y)$		$2680^+, 1424^+, -$	$23^+, 23^+, 23^+, 0.3^+$

Resolution is quoted in terms of the wire length HWA or the interrogation region size $\Delta W_{x,y}$ and light sheet thickness ΔW_z for PIV. The sampling interval for HWA or inter-frame time for PIV is given as Δt

†Interrogation window depth based on assumed laser-sheet thickness of 1 mm

Using time-resolved planar PIV measurements in a water tunnel Dennis and Nickels [4] used the space-time correlation $R_{u'u'}(\Delta x, \Delta t)$ at a height of $y = 0.16\delta$ to estimate the mean convection velocity across all resolved scales, in a turbulent boundary layer ($Re_\theta = 4685$). This mean convection velocity was approximately 1.8 % higher than the local mean velocity, however the effect of spatial resolution and the relative convection of different scales, were not investigated. LeHew et al. [11] performed similar measurements in a turbulent boundary layer to estimate the three-dimensional (3D) $\Phi(k_x, k_z, \omega)$ power spectra, enabling the calculation of k_x, k_z dependent convection velocities. From examination of the 3D $\Phi(k_x, k_z, \omega)$ spectra LeHew et al. [11] reported that at a wall-normal height of $y^+ = 34$, most scales travel slower than the local mean velocity, with the exception of the largest scales or smallest wave-numbers $1.2 < k_x\delta < 3$. These results ran counter to those derived from a linear fit to the local maximum in the premultiplied two-dimensional (2D) $k_x\omega\phi(k_x, \omega)$ spectrum, which instead indicated that most-scales convected at a velocity greater than the local mean with convection velocity increasing with streamwise wave-number.

The results of LeHew et al.'s [11] analysis, based on the spectra $\Phi(k_x, k_z, \omega)$, are more in-line with those of Krogstad et al. [9], who used the correlation of temporal signals from streamwise displaced HWAs to investigate the influence of streamwise scale over a range of $3.9 < k_x\delta < 314$ in a zero-pressure gradient boundary layer ($Re_\theta = 1409$) at multiple wall-normal positions. While the results of Krogstad et al. [9] show some sensitivity to the varying HWA probes used in that study, a similar trend of decreasing convection velocity is reported for increasing wave-number with only streamwise wave-numbers $k_x\delta < 32$ convecting at velocities greater than the local mean velocity at a height of $y^+ \approx 34$, compared to $k_x\delta < 3$ for LeHew et al. [11]. By considering multiple wall-normal positions Krogstad et al. [9] also show that while the trend towards lower convection velocities for higher wave-numbers and smaller-scales persists at almost all wall-normal positions, the relative convection velocity of a given scale, with respect to the local mean velocity, does not. Results showed that near the wall all scales appear to converge to a convection velocity

of approximately $U_c \approx 10.6^+$ with most scales convecting faster than the local mean for $y^+ < 70$ and most lower than the local mean velocity throughout the rest of the log layer and wake regions.

The discrepancy observed in the convection velocities derived from the 3D and 2D spectra of LeHew et al. [11] likely stem from the difficulty in calculating spectra from PIV data, which have been shown to be very sensitive to measurement noise [1, 6] and the number of velocity vectors over which they are calculated. de Kat et al. [2] investigated the influence of spatial and temporal resolution on the experimental investigation of turbulent convection velocity and suggested that the use of a phase-spectrum or the phase of the cross-spectrum between experimental PIV data at times t and $t + \Delta t$ can provide better estimates of the k_x dependent convection velocity than methods based on the calculation of the 2D $\phi(k_x, \omega)$ spectrum. Applying this methodology to a turbulent boundary layer ($\mathrm{Re}_\theta = 1409$) at $y/\delta = 0.1$, de Kat et al. [2] reported that the local mean velocity was the most likely convection velocity for scales in the range of $1 < k_x\delta < 80$, in contrast to the findings of LeHew et al. [11] and Krogstad et al. [9].

Recently del Álamo and Jiménez [3] performed direct numerical simulations (DNS) to generate a spatial and temporal record of the velocities in a turbulent channel flow at $\mathrm{Re}_\tau = 185$-1901, in order to investigate the convection of turbulent eddies. As in the boundary layer results of Krogstad et al. [9] the mean convection velocity was observed to be higher than the local mean near the wall, approaching a value of $U_c \approx 9^+$ at the wall. While it is natural to expect that the channel and boundary layer would behave in a similar manner near the wall, this convection value is lower than that reported by Krogstad et al. [9] for the boundary layer, $U_c \approx 10.6^+$, possibly due to the limitation in the smallest HWA separation used in the experiment. Results for the channel flow indicate that the small-scale eddies tend to follow the local mean velocity, while large-scale features propagate with a velocity much closer to that of the bulk flow or mean flow velocity across the channel height. This tendency for large-scales to converge to a convection velocity below the local mean is not observed in the HWA or PIV measurements of turbulent boundary layers discussed above. It is not yet clear if this is due to a fundamental difference between the convection of flow in a boundary layer and a channel, or if such an effect only occurs at scales beyond the spatial dynamic range of existing measurements. In the case of channel flow del Álamo and Jiménez [3] demonstrate that failure to account for the variation in convection velocity with scale can result in the erroneous conversion of temporal to spatial energy spectra and may be partially responsible for the observation of bimodal energy spectra in high Reynolds number wall-bounded flows [10].

In this paper turbulent convection velocities in a turbulent boundary layer are investigated using high repetition rate PIV measurements (HR-PIV) undertaken in a large horizontal water tunnel with a high temporal and spatial resolution. The noise-limited spatial and temporal dynamic range of the present measurement are estimated via the comparison of the measured spatial and temporal velocity power spectra with those of direct numerical simulation data, filtered at the same resolution as the present PIV measurement. Convection velocities are estimated using both the space-time correlation approach followed by Dennis and Nickels [4] and the phase-spectrum approach of de Kat et al. [2], in order to access both the mean and streamwise scale dependent convection velocities. Finally, the extent to which Taylor's hypothesis and a single mean convection velocity can be used to reconstruct a spatial field from temporally resolved data are evaluated over a range of wall-normal heights in a turbulent boundary layer.

2 Experimental Setup

Experiments were performed in a streamwise, wall-normal ($x-y$) plane spanning the buffer, logarithmic and wake layers of a turbulent boundary layer, formed on the floor of the 0.5 × 0.5 m cross-section horizontal water tunnel at the Laboratory for Turbulence Research in Aerospace and Combustion at Monash University. The boundary layer was tripped using a spanwise cylindrical rod with the addition of a trailing sandpaper element to provide a three-dimensional transition at the outlet of the contraction, as discussed in Herpin et al. [7]. HR-PIV measurements were performed approximately 4 m downstream of the trip, resulting in a boundary layer thickness of $\delta = 38.6$ mm with a momentum thickness based Reynolds number of $\mathrm{Re}_\theta = 2,250$ and a friction velocity based Reynolds number of $\mathrm{Re}_\tau = 840$.

In order to provide a field of view large enough to capture streamwise wavelengths over one boundary layer thickness, without sacrificing the resolution of the smaller scales, experiments were performed using two high-speed PCO. DiMax CMOS cameras (2016 × 2016 pixel each), aligned with a small overlap in the longitudinal direction. Illumination was provided by the use of a 60 mJ Quantronix Darwin Duo Nd:YLF laser collimated into a 1 mm light sheet and pulsed to enable a recording rate of 1.25 kHz. At this rate successive single shutter images enabled the calculation of velocity fields with a mean particle displacement of approximately 10 pixels at a temporal resolution of 0.8 ms or $0.03\nu/u_\tau^2$. Seeding was provided in the form of Potters hollow glass spheres with a mean diameter of 11 μm and a specific gravity of 1.1. The field of view and spatial resolution associated with this measurement are summarized in Table 1 and indicate a significantly higher resolution than that of Dennis and Nickels [4] and LeHew et al. [11] and higher temporal resolution than de Kat et al. [2].

Velocity fields were calculated using a multi-grid PIV algorithm [16] with window deformation [8, 13] and an initial and final interrogation window size of 64 × 64 and 32 × 32 pixels, respectively. A window overlap of 50 % was applied to the final pass. Vector validation was performed using normalized median vector validation [19] in both space and time. Five sets of 6305 vector fields were recorded, corresponding to the maximum available onboard memory in each camera. In order to provide a single high resolution and large field of view measurement, the individual velocity fields from each camera were merged in the streamwise direction by imposing a sharp transition in the middle of the overlap region, after de-warping the velocity fields from each camera using a standard polynomial calibration [15]. Further parameters associated with the PIV analysis are given in Table 2. Figure 1 provides an example of the raw merged velocity fields and the merged fields after filtering the measurement noise, as discussed in Section 3. The velocity profiles for both the raw and filtered fields are shown in Fig. 2.

Table 2 Parameters of the HR-PIV boundary layer measurements

Boundary layer thickness	$\delta^+ = 840$
Friction velocity	$u_\tau = 0.018$ ms^{-1}
Magnification	0.33
Spatial resolution	30.0 pixels/mm
Lens aperture	$f_\# = 4$
Particle image diameter	$d_p \approx 1$ pixel
Depth of field	$\Delta z \approx 0.7$ mm
Light-sheet thickness	$\Delta z = 1$ mm
Kinematic viscosity	$\nu = 8.42 \times 10^{-7}$ m^2/ s

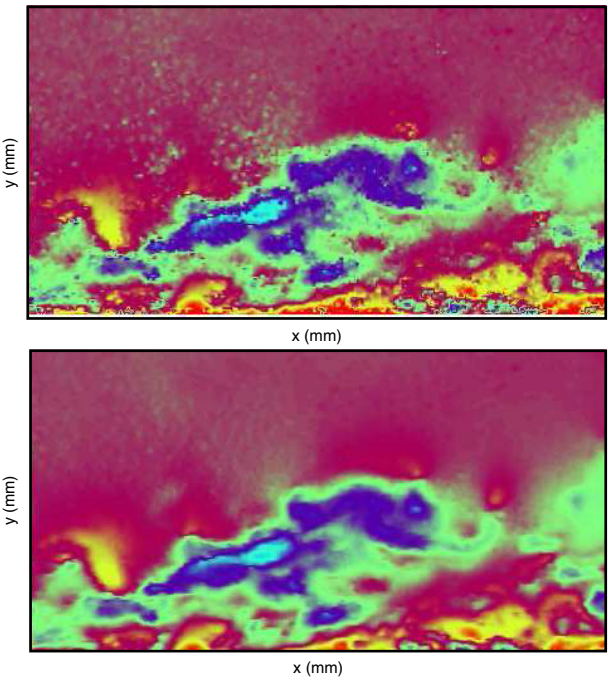

Fig. 1 Instantaneous iso-contours of the streamwise velocity fluctuations in the HR-PIV measurements of a turbulent boundary layer after merging velocity fields: (*top*) raw velocity field data; (*bottom*) temporally and spatially filtered velocity field

3 Determining the Noise-Limited Dynamic Range of the PIV Measurement

HR-PIV is capable of providing experimental measurements of both the spatial and temporal evolution of a turbulent flow, however it is important to recognize the influence of measurement noise on both the spatial and temporal dynamic range of such data. In theory the spatial dynamic range of PIV measurements are limited by the field of view, the interrogation window dimensions ΔW_x, ΔW_y and the light sheet thickness (in this case denoted as the effective interrogation window size in the spanwise direction ΔW_z). The temporal dynamic range is similarly limited by the number of images that can be recorded by the camera and the maximum recording rate or inter-frame times Δt of both the cameras and the laser. In practice the presence of measurement noise in a given PIV measurement means that the smallest scale that is accurately measured in the PIV measurement is generally larger than the cut-off associated with the chosen interrogation window size or inter-frame time [6]. An effective noise limited cut-off can be defined in both the spatial and temporal spectra as the wave-number or wavelength where the signal to noise ratio is equal to unity. Beyond this point the true turbulent signal cannot be distinguished from the measurement noise. This measurement noise is often masked by the spatial filtering of PIV such that the influence of measurement noise is often underestimated unless the spatial filtering of the measurement is taken into account [1]. A brief explanation of the methodology used to identify the noise limit is provided below. A more detailed explanation of this method can be found in Atkinson et al. [1].

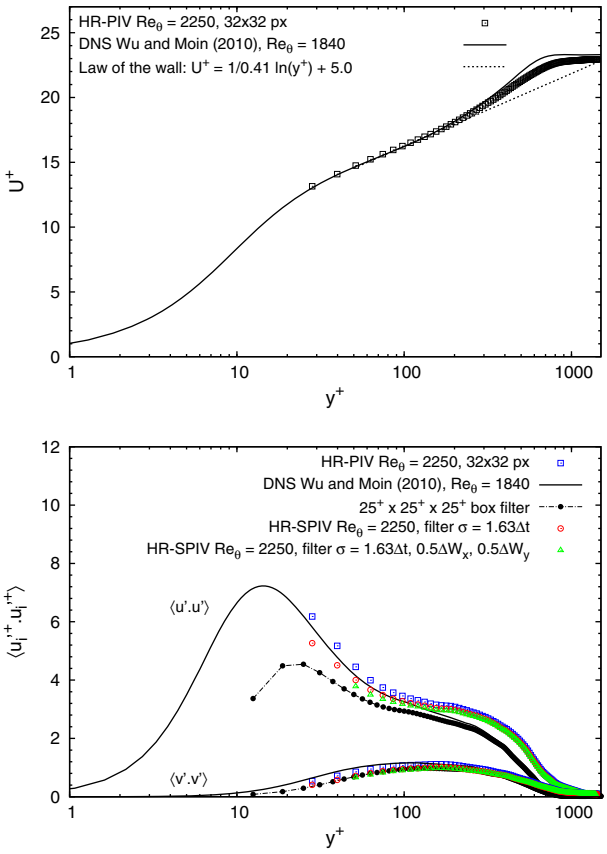

Fig. 2 Mean and wall-normal velocity and Reynolds stress profiles for the HR-PIV measurements of a turbulent boundary layer

In order to reduce the influence of measurement noise on the estimation of the convection velocity and to quantify the effective noise-limited spatial and temporal dynamic range of the present data, the temporal and spatial longitudinal velocity power spectra are examined after treating the data for periodicity as discussed in Foucaut et al. [6]. Figure 3 shows the influence of white-noise on the temporal spectra of the unfiltered HR-PIV spectra taken at $y^+ = 100$. In the absence of a temporal DNS spectra at the same spatial resolution as the PIV, the noise-limited temporal frequency $\omega_{\max}$ was determined following Foucaut et al. [6], where $\omega_{\max}$ is defined as the frequency at which the signal to noise ratio SNR = 1, $S_{11\,PIV}$ is the spectra obtained from PIV and $S_{11\,flow}$ is the true spectra of the flow, or in this case the spectra obtained from the DNS:

$$S_{11\,PIV}(\omega_{\max}) = 2S_{11\,flow}(\omega_{\max})\left(\frac{\sin \omega_{\max}\Delta t/2}{\omega_{\max}\Delta t/2}\right)^2 \tag{2}$$

To reduce the influence of measurement noise at frequencies greater than $\omega_{\max}$ the HR-PIV velocity field was spatially filtered using an 11 point Gaussian kernel in the temporal domain with $\sigma_t = 1.63\Delta t$, which provides a -3 dB cut-off at $\omega_{\max}\Delta t \approx 0.51$, which is approximately where noise begins to dominate the temporal spectra.

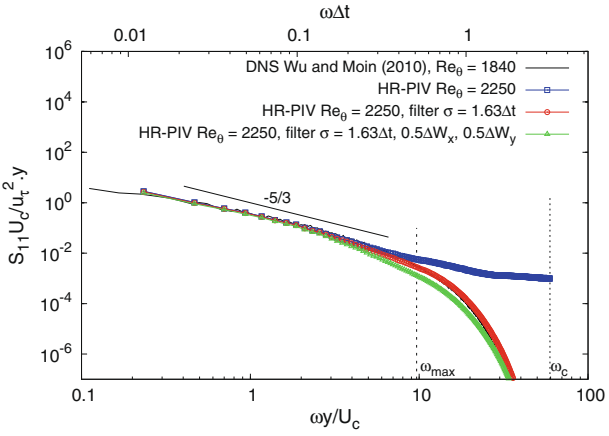

Fig. 3 Temporal velocity power spectra at $y^+ = 100$ for HR-PIV measurements of a turbulent boundary layer at $\mathrm{Re}_\theta = 2,250$ and DNS of Wu and Moin [21] at $\mathrm{Re}_\theta = 1840$. Temporal spectra is calculated over a domain of only $240\Delta t$. U_c is the convection velocity assumed to be equal to the local mean velocity

Figure 4 shows the influence of temporal filtering on the spatial velocity power spectra, bringing the experimental data more in line with the DNS spectra. However, it should be noted that the experimental spectra still peals away from the DNS when it is box filtered with interrogation window dimensions similar to that of the present PIV measurement. This dashed spectra represents the spectra that should be provided by the HR-PIV measurement in the absence of measurement noise. Following the methodology in Atkinson et al. [1], which accounts for the influence of spatial filtering on PIV, the noise-limited spatial wavenumber $k_{\max}$ can be estimated as:

$$E_{11\,PIV}\left(k_{\max\,1\mathrm{D}}\right) \approx 2E_{11\,filt}\left(k_{\max\,1\mathrm{D}}\right) \tag{3}$$

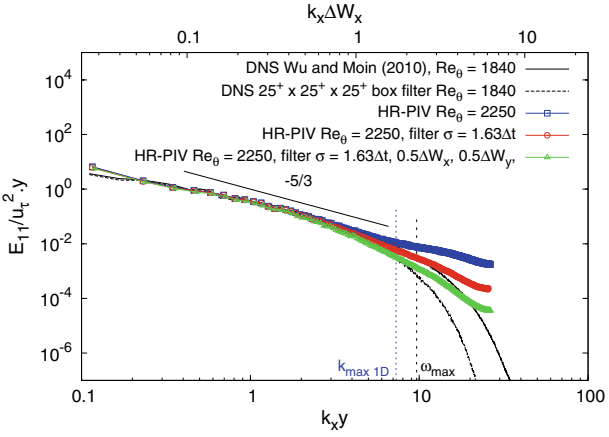

Fig. 4 Spatial velocity power spectra at $y^+ = 100$ for HR-PIV measurements of a turbulent boundary layer at $\mathrm{Re}_\theta = 2,250$ and DNS of Wu and Moin [21] at $\mathrm{Re}_\theta = 1840$

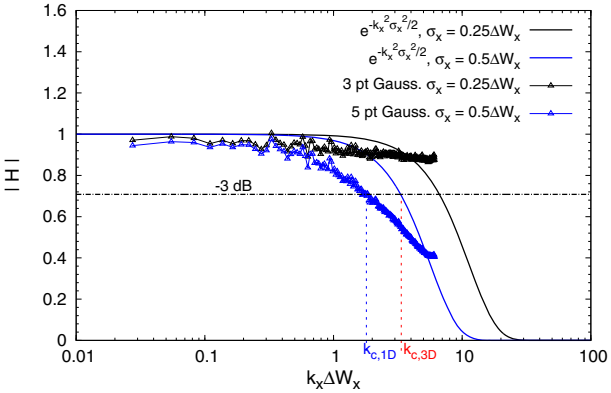

Fig. 5 Apparent 1D transfer function associated with the 2D Gaussian filtering of HR-PIV data of a turbulent boundary layer at $\mathrm{Re}_\theta = 2,250$ at $\mathrm{y}^+ = 100$

where $E_{11\,filt}(k_x)$ is the spectrum of the DNS after filtering at the resolution of the PIV. In this case 2D Gaussian filtering in the x and y directions with a five point kernel and $\sigma_{x,y} = 0.5\Delta W_{x,y}$ provides a -3 dB cut-off at $k_{\max 1D}\Delta W_x \approx 1.73$ in the 1D spectra. Owing to the 1D representation of a 2D filter this cut-off corresponds to a 3D cut-off of $k_{\max}\Delta W_x \approx 3.36$. This is due to the difference in the true 2D and apparent 1D transfer functions of the filter as shown in Fig. 5. Again, a detailed explanation of this behavior can be found in Atkinson et al. [1].

The effect of the combined temporal and spatial filtering can be observed in both the iso-contours of the instantaneous velocity field (see Fig. 1) and the Reynolds stress-profiles (see Fig. 2), where filtering reduces the fluctuations to a level more inline with those of the noise-free spatially filtered DNS. The theoretical and noise-limited temporal and one-dimensional spatial dynamic range of the current measurement are given in Table 3. Assuming the noise-level in the spectra is independent of wall-height the relative noise-limited wave-numbers will decrease with height above the wall as the energy level in the turbulent fluctuations is reduced, relative to a constant background noise. Figure 6 shows the effective noise limited waves-numbers as a function of wall-height, based on the energy level of the noise identified at $y^+ = 100$. While, scales at wave-numbers higher than the cut-offs shown are not captured by the measurement and will not contribute to the results in discussed in Section 4, the same is not true for the lower wave-numbers. Wave-numbers below those shown in Table 3 cannot be individually resolved due to the field of view of the present measurement, however being an experimental observation of a physical flow, the influence of these scales will still be present in the mean convection velocities.

Table 3 Temporal and spatial dynamic range of the HR-PIV boundary layer measurements at $y^+ = 100$

Domain		Theoretical	Noise-limited
Spatial	$k_x\Delta W_x$	$0.056 - 3.1$	$0.056 - 1.7$
	$k_x\nu/u_\tau$	$0.002 - 0.14$	$0.002 - 0.075$
Temporal	$\omega\Delta t$	$0.001 - 3.1$	$0.001 - 0.51$
	$\omega\nu/u_\tau^2$	$0.003 - 10$	$0.003 - 1.7$

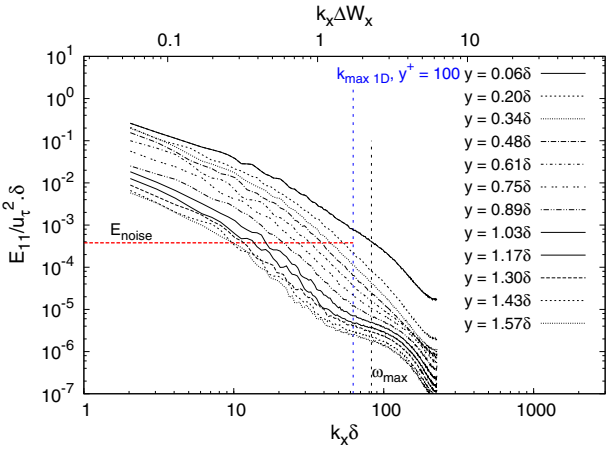

Fig. 6 Noise-limited wave-number at different wall heights in the HR-PIV data of a turbulent boundary layer at $\mathrm{Re}_\theta = 2,250$ relative to the spectral energy content of the measurements noise at $y^+ = 100$

4 Mean Convection Velocities

In order to obtain the mean convection velocity for all scales (k_x, k_z) in a turbulent boundary layer, over a range of wall-normal positions, the space-time correlations were obtained by two-point correlation of the streamwise and wall-normal velocity components of the filtered HR-PIV data as follows:

$$R_{u'u'}(dx, y, dt) = \frac{\langle u'(x, y, t) \cdot u'(x + dx, y, t + dt) \rangle}{\sigma'_u(y) \cdot \sigma'_u(y)} \tag{4}$$

where u' denotes the fluctuating velocity component and dx and dt are the relative offsets in the streamwise and temporal directions, respectively. Each point in the space-time correlation represents the ensemble of over 4.5 million points, such that the uncertainty associated

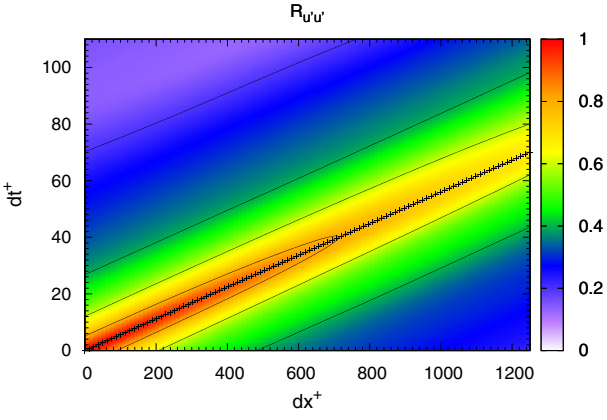

Fig. 7 Space-time correlation of the streamwise velocity fluctuations at $y^+ = 170$ calculated from HR-PIV data of a turbulent boundary layer at $\mathrm{Re}_\theta = 2,250$

with the correlation map was negligible. Figure 7 shows an example of the space-time correlation function at $y/\delta \approx 0.2$ or $y^+ \approx 170$, indicating that on average the streamwise velocity fluctuations maintain a correlation coefficient $R_{u'u'} > 0.6$ over a distance of almost 2δ at this height. The degree to which such a correlation is maintained is discussed further in Section 6.

As in the approach of Dennis and Nickels [4] the convection velocity can be obtained by fitting a line to the maximum in the space-time correlation, whose gradient represents the mean convection velocity for all scales present in the experimental flow, down to the measurement noise cut-off. For the present measurements this fit was applied to the location of the peak correlation in dt for a given spatial offset dx, detected via a three-point Gaussian peak fit to the correlation function, as typically used to find the correlation peak to sub-pixel accuracy in cross-correlation based PIV algorithms. In all cases the linear fit resulted in a regression coefficient greater than 0.99, resulting in a 95 % confidence interval in the gradient of the linear fit on the order of the marker size shown in subsequent figures.

The variation in the mean convection velocity $\langle U_c \rangle$ with wall height is shown in Fig. 8. These results indicate convection velocities greater than the local mean velocity for wall heights $y^+ < 300$ or $y < 0.35\delta$ and lower than the local mean for regions above this. Dennis and Nickels [4] also report a mean convection velocity greater than the local mean at $y = 0.18\delta$. At this height Dennis and Nickels [4] report a convection velocity 1.8 % greater than the local mean, compared to 1.3 % greater than the local mean at $y = 0.2\delta$ in the present experiment. This difference will in part be due to the variation in wall normal position, but may also be influenced by variation in the resolution of the two measurements. From this single wall-normal position [4] conclude that the convection velocity is close to the local mean, however present results indicate a more interesting relationship between the convection velocity and the local mean that differs with wall-normal position. The results of Krogstad et al. [9] present convection velocities for different streamwise scales, rather than an overall mean, yet also indicate convection velocities higher than the local mean for $y^+ < 70$. Above this height Krogstad et al.'s [9] results show most scales convecting slower than the local mean, suggesting that the mean convection velocity would also be lower than the local mean.

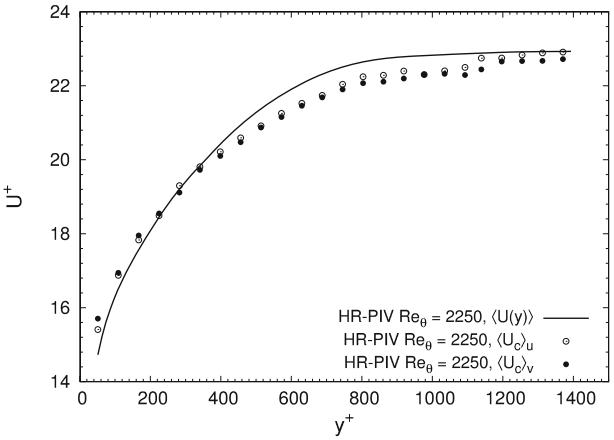

Fig. 8 Mean convection velocity at various heights above the wall as calculated from space-time correlation of u' and v' using HR-PIV data of a turbulent boundary layer at $\mathrm{Re}_\theta = 2,250$. Local mean velocity is shown for comparison

Mean convection velocities higher than the local mean in the viscous and buffer layer and lower than the mean in the logarithmic and wake regions were also observed by del Álamo and Jiménez [3] in turbulent channel flows. In the channel DNS this cross-over in the convection velocity, relative to the local mean, occurs at a much lower wall-normal position with mean convection velocities dropping below the local mean velocity for $y^+ > 15$ when all scales are considered. del Álamo and Jiménez [3] also show that this cross-over varies significantly with wave-number, increasing to $y > 0.2\delta$ when only scales greater than twice the channel height are considered. The limited spatial resolution of the present measurement is likely to be at least partially responsible for the high cross-over in the mean convection velocities shown in Fig. 8, however this cross-over remains considerably higher than that which would be expected for the channel at the same spatial resolution. This suggests that convection velocities higher than the local mean persist at higher wall-normal positions in the boundary layer than in in the channel, possibly due to differences in the interaction between the inner and outer flows in each case.

Comparison of the space-time correlations and mean convection velocities for both the streamwise u' and wall-normal v' velocity fluctuations show higher convection velocities for the v' fluctuations near the wall and lower velocities, relative to the u' fluctuations, at the top of the boundary layer. This difference is consistent with the channel flow DNS results of del Álamo and Jiménez [3]. Within the spatial resolution limits of the present experiment the average convection velocity across the resolved scales is shown to vary from the local mean by up to 3.5 % in the wake region. Interestingly the u' fluctuations convect at velocities lower than the free-stream velocity up to a height of approximately 1.5δ ($y^+ \approx 1200$), which is consistent with the upper bound of the instantaneous position of the turbulent / non-turbulent interface, representing the boundary between rotational and irrotational flow at the upper limit of the boundary layer. A similar increase is observed in the mean convection velocity of the v' fluctuations, however the mean convection velocity remains lower than the free-stream velocity up to 2δ. Similar computation of mean convection velocities on the unfiltered PIV data produced negligible difference in the results, indicating that the filtering used did not remove any meaningful scales from the measurement.

5 Wave-Number Dependent Convection Velocities

To examine the variation in convection velocity as a function of streamwise wave-number k_x, the scale-dependent convection velocity was calculated from the phase-spectrum or the phase angle of the cross-spectra between velocity fluctuations at times t and $t + \Delta t$, following:

$$u_c(k_x, y, t) = \frac{\langle \Psi(k_x, y, t) \rangle}{k_x \cdot \Delta t}, \tag{5}$$

where $\Psi(k_x, y, t)$ is the phase-spectrum. The results of de Kat et al. [2] indicate that this method is less susceptible to measurement noise and limited fields of view which can otherwise influence the calculation of the 2D $\phi(k_x, \omega)$ spectrum.

Figure 9 shows the convection velocity at different heights above the wall as a function of the streamwise wave-number k_x, averaged across all resolved spanwise wave-numbers k_z and normalized by the local mean velocity at each height. In order to limit the influence of measurement noise the phase-spectra at each height were truncated at the streamwise wave-number beyond which the energy in the spectra drops below the noise level of the present measurement, as depicted by the line in Fig. 6. Results indicate a decrease in convection velocity with increasing wave-number over the entire range of wall-normal heights captured

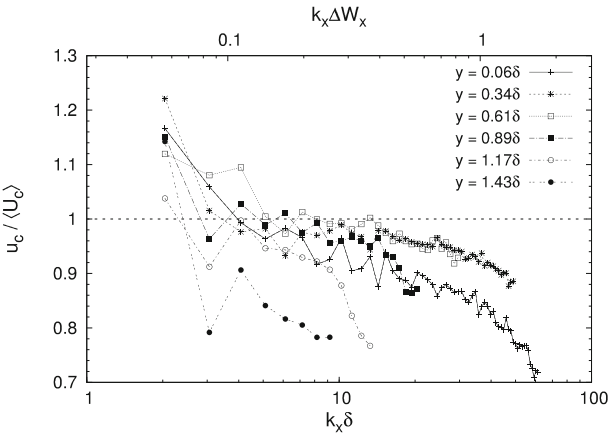

Fig. 9 Convection velocity as a function of streamwise wave-number at various heights above the wall as calculated from the phase-spectra of the HR-PIV data at times t and $t + \Delta t$. Convection velocities are calculated for the streamwise u' fluctuations and normalized by the local mean convection velocity

in the present measurement ($y^+ = 30$ to $y = 1.7\delta$). The 3D $\Phi(k_x, k_z, \omega)$ convection velocities of LeHew et al. [11] at $y^+ = 34$ and Krogstad et al.'s [9] boundary layer measurements show a similar trend of increasing convection velocity for increasing streamwise flow scale, up to the largest measured scale $k_x\delta = 3.9$. The exception to this is the viscous and lower buffer layer $y^+ < 10$, where Krogstad et al. [9] shows an increase in the convection velocity of the smallest scales, however this cannot be tested with the current data set.

In channel flows, del Álamo and Jiménez [3] report that the smallest scales convect at velocities close to the local mean while the largest scales convect with a velocity closer to the bulk velocity in the channel. This does not appear to be the case in the current boundary layer data or that of Krogstad et al. [9], where in both cases the smallest streamwise scales convect at velocities well below the local mean. It is possible that this difference is a consequence of not accounting for variation in the spanwise scales. For spanwise scales $k_z\delta < 25$ and over a similar range of streamwise scales to the present experiment $6.3 < k_x\delta < 105$, del Álamo and Jiménez [3] also show a decrease in convection velocity with increasing wave-number. For wave-number below this, del Álamo and Jiménez [3] show that the convection velocity begins to decreases again towards the bulk velocity. This is not observed in the present measurement for wave-numbers down to $k_x\delta = 2$, indicating that if the largest scales in the boundary layer approach a similar wall-normal mean or bulk velocity, they only approach this velocity at scales larger than those in the channel flow and beyond the range of the present measurement.

6 Validity of Taylor's Hypothesis Using Scale-Independent Convection Velocities

In the following the validity of Taylor's hypothesis is assessed using a scale-independent convection velocity as it is used in most practical applications (e.g. HWA) where temporal spectra are converted into spatial spectra. For this, the spatial velocity field is reconstructed from the temporal data at a single location and compared to the measured instantaneous spatial field using either the local mean or the scale-averaged convection velocity computed in Section 4.

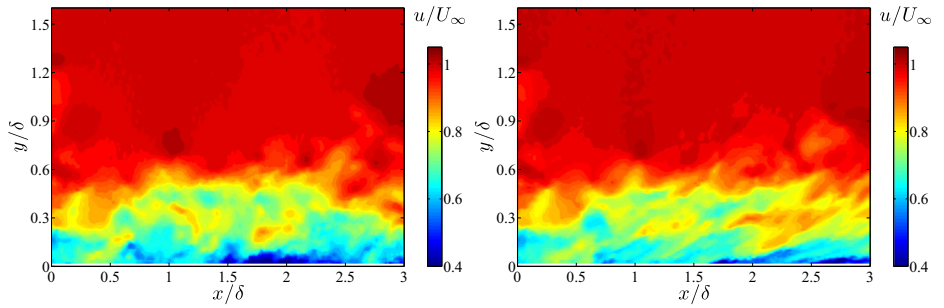

Fig. 10 Example of the instantaneous spatial velocity field u/U_∞: (*left*) measured by HR-PIV; (*right*) reconstructed using Taylor's hypothesis and the scale-averaged convection velocity $\langle u_c \rangle$

Figure 10 provides an example of the instantaneous spatial velocity field measured by PIV and that produced by applying Taylor's hypothesis using the scale-averaged convection velocity. A good qualitative agreement between the two velocity fields can be observed up

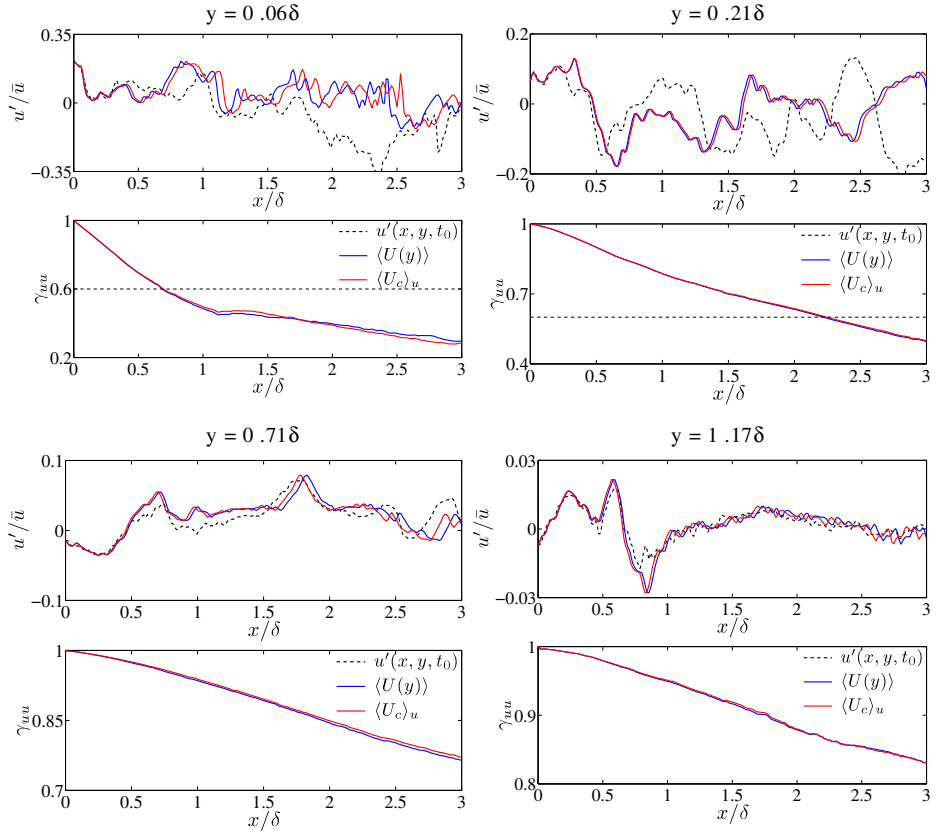

Fig. 11 Comparison between the measured and reconstructed fluctuating velocity field u'/u_∞ at various heights above the wall using the local mean and the scale-averaged convection velocity in the Taylor's approximation

to a streamwise distance of 0.5–1.0 δ depending on wall-normal position. For projection distances larger than $\sim \delta$ an appreciable difference exists, particularly for the near-wall flow region as seen in Fig. 11. In addition, the turbulent structures are sheared due to the variable convection velocity in the wall-normal direction indicating that a scale-independent convection velocity is no longer valid in this region. In the wake region (Fig. 11), where the convection velocity is nearly constant and the velocity fluctuations are small, Taylor's hypothesis seems to hold reasonably well over long distances ($> 3\delta$).

In order to quantify the limits of Taylor's hypothesis the cross-correlation between the instantaneous and corresponding reconstructed spatial Taylor fields was calculated. The Taylor fields were reconstructed over approximately 600 time steps corresponding to approximately three eddy-turnover times (tU_∞/δ) and subsequently interpolated onto an equidistance grid to match the vector spacing of the experiment. The resulting correlation coefficients $\gamma_{uu}(x)$ and $\gamma_{vv}(x)$, for the streamwise and wall-normal velocity fluctuations, are shown in Fig. 12 as a function of wall-normal position. These correlation coefficients decrease with streamwise distance and represent the increasing variation between the measured and reconstructed velocity fields due to the meandering flow motion, Lagrangian turbulent fluctuations and the scale-dependent convection velocities. For example, at a

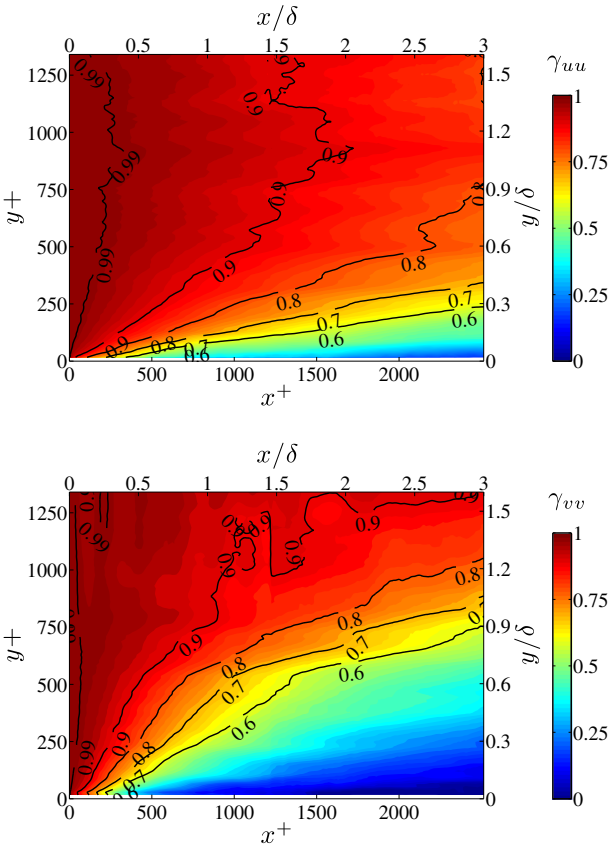

Fig. 12 Cross-correlation coefficient γ_{uu} (*top*) and γ_{vv} (*bottom*) between the instantaneously measured and reconstructed spatial velocity field. The scale-averaged convection velocities $\langle u_c \rangle_u$ and $\langle u_c \rangle_v$ are used for Taylor's approximation

wall-normal height of 0.21δ ($y^+ = 176$) γ_{uu} decreases to 0.6 after a convection distance of approximately 2δ. This corresponds to an equivalent convection time of $tU_\infty/\delta = 2$ (or $t^+ \approx 75$). For the vertical v' fluctuations, the correlation coefficient γ_{vv} has already decreased below 25 % over the same convection distance. These results show that over most wall-normal positions Taylor's hypothesis breaks down far more rapidly for the wall-normal velocity component than for the streamwise component.

A similar behaviour can be observed if the local mean velocity is used as the convection velocity with only a marginal difference in the correlation coefficient across the boundary layer height as shown in Fig. 11. Similar results were obtained by Dennis and Nickel [4] who used a scale-averaged convection velocity and Schröder et al. [14] who assumed the local mean streamwise velocity as the appropriate convection velocity, albeit over a smaller range of wall-normal positions. The use of scale mean convection velocity was only found to provide a better approximation to the true velocity field for convection distances $\geq \delta$, at which point the validity of any single scale independent convection velocity becomes questionable.

7 Conclusion

Experiments were performed in a water tunnel using high repetition rate PIV in order to investigate the convection velocity in a turbulent boundary layer over a wide range of wall-normal positions from $y = 0.06\delta$–1.6δ. Multiple cameras were used to improve the spatial dynamic range of the measurement and enable the investigation of a broader range of scales in the flow. To restrict the influence of measurement noise and quantify the effective noise-limited spatial and temporal dynamic range of the measurement, an extensive validation was performed via comparison with spatially filtered DNS data. Space-time correlations indicated mean convection velocities for both streamwise and wall-normal velocity fluctuations that are greater than the local mean velocity for wall heights $y^+ < 300$ or $y < 0.35\delta$, and less than the local mean velocity with a convection velocity approximately 3.5 % lower than the local mean convection velocity until beyond the upper bound of the turbulent non-turbulent interface $y > 1.5\delta$. The convection velocities of different streamwise length scales were examined via the use of the velocity phase-spectra. The convection velocity was observed to decrease with increasing wave-numbers for all wall-normal positions considered. These trends in convection velocity are consistent with earlier HWA based boundary layer measurements of Krogstad et al. [9]. Despite differences between the nature of boundary layer and channel flows, the observed behavior of the convection velocity in the present boundary layer investigation is similar to that reported by del Álamo and Jiménez [3] in their turbulent channel flow DNS, however several differences were observed. Present results, and those of Krogstad et al. [9], indicate that the mean convection velocities in a turbulent boundary layer remains higher than the local mean velocity for greater heights above the wall and do not begin to converge towards a bulk velocity at the same scales as the channel.

Comparison between the measured and reconstructed spatial fields show that the streamwise extent over which Taylor's hypothesis can be applied, increases with wall-normal locations when using the local mean or scale-averaged convection velocity. Close to the wall, where turbulent fluctuations are strongest, Taylor's hypothesis is limited to streamwise distances $< \delta$. In the wake region of the turbulent boundary layer, Taylor's hypothesis holds over at least 3δ. Interestingly these results show significant differences between

the application of Taylor's hypothesis to streamwise and wall-normal velocity fluctuations, posing more stringent restrictions on Taylor's hypothesis for the wall-normal velocity component.

Acknowledgments The support of Australian Research Council for this work is gratefully acknowledged. Our thanks to Associate Professor Xiaohua Wu for graciously providing the DNS velocity fields that were used to establish the noise limited wavenumbers in our experimental study.

References

1. Atkinson, C., Buchmann, N.A., Amili, O., Soria, J.: On the appropriate filtering of PIV measurements of turbulent shear flows. Experiments in Fluids **55**(1), 1–15 (2013)
2. de Kat, R., Gan, L., Dawson, J.R., Ganapathisubramani, B.: Limitations of estimating turbulent convection velocities from PIV. In: 16th Int. Symp. App. Laser Techniques to fluid Mech., Lisbon, Portugal, 9-12 July (2012)
3. del Álamo, J.C., Jiménez, J.: Estimation of turbulent convection velocities and corrections to Taylor's approximation. J. Fluid Mech. **640**, 5–26 (2009)
4. Dennis, D.J.C., Nickels, T.B.: On the limitations of Taylor's hypothesis in constructing long structures in a turbulent boundary layer. J. Fluid Mech. **614**, 197–206 (2008)
5. Dennis, D.J.C., Nickels, T.B.: Experimental measurement of large-scale three-dimensional structures in a turbulent boundary layer. part 2. long structures. J. Fluid Mech. **673**, 218–244 (2011)
6. Foucaut, J.M., Carlier, J., Stanislas, M.: PIV optimization for the study of turbulent flow using spectral analysis. Meas. Sci. Technol. **15**, 1046–1058 (2004)
7. Herpin, S., Wong, C.Y., Stanislas, M., Soria, J.: Stereoscopic PIV measurements of a turbulent boundary layer with a large spatial dynamic range. Exp. Fluids **45**, 745–763 (2008)
8. Huang, H.T., Fiedler, H.E., Wang, J.J.: Limitations and improvements of PIV; part II: particle image distortion, a novel technique. Exp. Fluids **15**, 263–273 (1993)
9. Krogstad, P., Kaspersen, J.H., Rimestad, S.: Convection velocities in a turbulent boundary layer. Phys. Fluids **10**(4), 949–957 (1998)
10. Kunkel, G.J., Marusic, I.: Study of the near-wall-turbulent region of the high-reynolds-number boundary layer using atmospheric data. J. Fluid Mech. **548**, 375–402 (2006)
11. LeHew, J., Guala, M., McKeon, B.J.: A study of the three-dimensional spectral energy distribution in a zero pressure gradient turbulent boundary layer. Exp. Fluids **51**, 997–1012 (2011)
12. Lin, C.C.: On Taylor's hypothesis and the acceleration terms in the navier-stokes equations. Q. Appl. Math. **10**(4), 295–306 (1953)
13. Scarano, F.: Iterative image deformation methods in PIV. Meas. Sci. Technol. **13**, R1-R19 (2002)
14. Schröder, A., Geisler, R., Staack, K., Elsinga, G.E., Scarano, F., Wieneke, B., Henning, A., Poelma, C., Westerweel, J.: Eulerian and lagrangian views of a turbulent boundary layer flow using time-resolved tomographic PIV. Exp. Fluids **50**, 1071–1091 (2011)
15. Soloff, S.M., Adrian, R.J., Liu, Z.C.: Distortion compensation for generalized stereoscopic particle image velocimetry. Meas. Sci. Technol. **8**, 144–1454 (1997)
16. Soria, J.: An investigation of the near wake of a circular cylinder using a video-based digital cross-correlation particle image velocimetry technique. Exp. Therm. Fluid Sci. **12**, 221–233 (1996)
17. Taylor, G.I.: The spectrum of turbulence. Proc. R. Soc. Lond. **164**(919), 476–490 (1938)
18. Townsend, A.A.: The structure of turbulent shear flows. Cambridge University Press, UK (1956)
19. Westerweel, J., Scarano, F.: Universal outlier detection for PIV data. Exp. Fluids **39**, 1096–1100 (2005)
20. Wills, J.A.B.: Convection velocities in turbulent shear flows. J. Fluid Mech. **20**, 417–432 (1964)
21. Wu, X., Moin, P.: Transitional and turbulent boundary layer with heat transfer. Phys. Fluids **22**, 085105 (2010)
22. Zaman, K.B.M.Q., Hussain, A.K.M.F.: Taylor's hypothesis and large-scale coherent structures. J. Fluid Mech. **112**, 379–396 (1981)